East African Journal of Biophysical and Computational Sciences
ISSN (Online): 2789-3618 and ISSN (Print): 2789-360X

ARTICLE

Computational Study of MHD Blood Flow through Bifurcated Artery Using Caputo-Fabrizio Fractional Derivative, Thermal Radiation, and Magnetic Field for Tumor Therapies

ARTICLE INFO
Volume 7(1), 2026
https://dx.doi.org/10.4314/eajbcs.v7i1.2S

ARTICLE HISTORY
Received: March 10, 2026
Accepted: 23 May, 2026
Published Online: 10 June, 2026

CITATION
Abdullahi et.al (2026). Computational Study of MHD Blood Flow through Bifurcated Artery Using Caputo-Fabrizio Fractional Derivative, Thermal Radiation, and Magnetic Field for Tumor Therapies. *East African Journal of Biophysical and Computational Sciences* Volume 7(1), 2026. .https://dx.doi.org/10.4314/eajbcs.v7i1.2S.18-26

OPEN ACCESS

Isah Abdullahi[1], Dauda Gulibur Yakubu[1,*], Muhammad Shamsuddeen Dauda[2], Mahmood Abdulhameed[3],Saidu Abubakar Kadas[4],Mohammed Abdulhameed[5], and Garba Tahiru Adamu[6]

[1]Department of Mathematical Sciences, Abubakar Tafawa Balewa University, Bauchi, Nigeria
[2]Department of Biological Sciences, Abubakar Tafawa Balewa University, Bauchi, Nigeria
[3]Department of Electrical Electronic Engineering, Abubakar Tafawa Balewa University, Bauchi, Nigeria
[4]Department of Obstetrics Gynaecology, ATBU, Teaching Hospital, Bauchi, Nigeria
[5]School of Science and Technology, The Federal Polytechnic Bauchi, Nigeria
[6]Department of Mathematical Sciences, Bauchi State University, Gadau, Bauchi, Nigeria

*Corresponding author: dgyakubu@atbu.edu.ng

Abstract

This study investigates the impact of heat sources, thermal radiation, and chemical reactions on the magnetohydrodynamic blood flow through a bifurcated artery in the presence of a slanted magnetic field. Using Laplace transform and the method of undetermined coefficients, the constitutive equations for the mathematical model of Caputo-Fabrizio fractional derivative order were solved. Blood flow velocity, temperature distribution, and concentration were found to have analytical expressions. The effects of certain physical parameters on blood velocity, temperature and concentration are graphically represented, and these representations accurately depict the flow disturbances. We discovered that the bifurcation apex of the artery with a symmetrical divider has steady blood flow. This may lead to significant shear stresses on either side of the bifurcation. Near the apex, when the flow is substantially different, obstruction may result from the formation of boundary layers on the inner walls of the bifurcation. Sluggish flow also occurred along the outer walls of the bifurcation. It has also been discovered that the temperature distribution, concentration, and arterial blood flow velocity are significantly influenced by the fractional order parameter, the slanted magnetic fields, the heat source, and the chemical reaction parameter. This study offers significant benefits for medical applications in biomechanical engineering, biomedical engineering, and medicine.

Keywords: Chemical reaction; Heat source; MHD Blood flow; Slanted magnetic field; Thermal radiation

1 Introduction

Bio-magnetic fluid dynamics (BFD), which is the study of bio-fluid flow in the presence of magnetic field, is a rapidly developing subject of study in fluid mechanics (Tzirtzilakis, 2005). This field of study is of tremendous importance to the field of medical science and has the possibility to be utilized in a diversity of domains, including the delivery of medications via the utilization of magnetized particles, the management of severe bleeding, and the assistance in dealing with malignant cancers (Shit & Majee, 2015). Understanding many facets (aspects) of the medical sciences, such as homeostasis, treating cancerous tumors, and administering medication using magnetic particles, depends on the study of biomagnetic fluid dynamics (Shaw & Murthy, 2010). Blood's hemoglobin molecules are regarded as biomagnetic fluids with magnetic properties. Blood can also be considered as a Newtonian fluid if it flows through the bigger arteries at a high shear rate. These arteries are thought to be homogenous whose flow behavior can be described by a Newtonian model (see, Caro et al., 2011; MacDonald, 1979). Numerous researchers have looked into various possibilities for studying physiological fluids

using porous media (see, Bhatti & Lu, 2019; Dash et al., 1996; Ramesh & Devakar, 2015; Shit & Roy, 2015) developed blood flow model via porous medium. Based on Darcy's law, Bhargava et al. (2007) and Ghasemi et al. (2015) investigated the pulsatile flow and mass transfer of an electrically conducting Newtonian bio-fluid via a channel comprising porous media using blood as the porous medium fluid. Bhatti et al. (2018) developed a mathematical model to investigate heat transfer, mass transfer, and blood flow in a porous medium channel while accounting for the integrated Darcy-Brinkman-Forchheimer model. Blood behaves non-Newtonian even in larger arteries at low shear rates, as demonstrated by Liepsch (1986). When blood flows through arteries at a low shear rate, it can be treated as Cassons fluid (Srivastava & Srivastava, 1984). Many researches have supported the Casson fluid model for blood flow via tiny arteries at low shear rates (see,Hayat et al., 2016; Nagarani et al., 2006; Venkatesan et al., 2013). Many authors (see, Abdulhameed et al., 2017; Misra & Shit, 2009; Mondal & Shit, 2017; Yakubu et al., 2020; Zeeshan et al., 2017) have regarded blood as a non-Newtonian fluid, because of its electrical conductivity, displays magneto hydrodynamic behavior.

Many authors considered the examination of the heat and mass transfer occurrences generated from these processes to be a highly relevant element with respect to modeling physiological processes (Prasad et al., 2025) and industrial processes (Sademaki et al., 2026). Electromagnetohydrodynamics is the study of fluids whose motion is constantly affected by externally applied magnetic field and electric field. In order to comprehend the impact of magnetohydrodynamic (MHD) and electrohydrodynamic (EHD) forces on the flow of normal fluids, including blood, several studies have mostly concentrated on the theoretical, computational, and experimental aspects of these forces. Cell-based therapies, medication delivery, and biological processes are just a few of the fields where the application of (EHD) has shown notable advancement. Additional force components, primarily the Lorentz and Coulomb forces, are incorporated into momentum equations and have a direct effect on fluid velocity. Magnetohydrodynamics or MHD has been used in a wide variety of biomedical applications (Vardanyan, 1973).

The heat transmission and magnetohydrodynamic (MHD) blood flow in a restricted artery were studied by Majee and Shit (2017). Akbar and Butt (2017) considered ferromagnetic blood flow in a restricted, smaller artery with a porous wall. The radiant heat transfer that takes place in the blood vessels must also be considered while treating hyperthermia. Oncology professionals are familiar with the medical practice of using heat therapy to cancer patients. Chinyoka and Makinde (2014) investigated the effects of magnetic fields and heat radiation on arterial blood flow. Sinha and Shit (2015) investigated the magnetic hydrodynamic blood flow in the presence of thermal radiation. Tabi et al. (2017) studied the combined effects of magnetic fields and external radiation on blood flow in the major blood arteries. Yakubu et al. (2022) examined blood flow of Oldroyd-B fluids in order to investigate the erratic flow, with magnetic field applied perpendicular to the flow direction. Heat transfer processes were studied in the peristaltic flow of blood with variable viscosity particle-liquid suspensions by Bhatti et al. (2016). Blood flow is greatly affected when the human body is exposed to a vibratory environment, as occurs when operating machines or traveling in spacecraft. When the human body undergoes body acceleration, a number of health problems might arise, such as an elevated heart rate and vision loss. In the study of the impact of body acceleration, a number of researches have produced mathematical simulations of oscillatory blood flow (see, Chaturani & Palanisamy, 1990; Ghasemi et al., 2016; Sud & Sekhon, 1984). Bhatti and Lu (2019) investigated the propagation of a hydro elastic single wave in a channel with uniform flow. Blood flow characteristics have been discovered to promote blood velocity in a vibratory environment using fractional order derivative differential equation problems. Fractional differential equations are the most used method for modeling natural phenomena. This is due to the fact that equations offer the possibility for a system to either retain memory or to be hereditary with the properties of its history, similar to how dynamic systems work (Syed et al., 2026).

Fractional order derivatives have been applied in many fields of study, including the complicated dynamics and rheological properties of different kinds of fluids. The behavior of fluid flow is well depicted by substituting fractional-order derivatives for the ordinary time derivative in the constitutive equations (see, Atangana and Baleanu, 2016; Caputo and Fabrizio, 2015; Samko et al., 1993). The concept of fractional calculus was initially proposed by L'Hôpital in 1695, more than four centuries ago. Therefore, it wasn't until the last few decades that a significant number of scholars started to highlight the fact that differential equations and fractional derivatives have numerous applications in a variety of domains (see, Abdulhameed et al., 2023; Imoro et al., 2024). These days, fractional derivative order differential equation problems are the most effective and successful ways to model the nonlinear processes that emerge in many domains of applied study, including biology, chemistry, ecology, engineering, and many other application areas. Several mathematical models have shown that they offer a more realistic depiction of the phenomenon under research. Examples of these models include those employed in biomedical engineering, viscoelastic mechanics, boundary layers, electromagnetic, and porous media. Bansi et al. (2018) investigated a fractional blood flow model in the oscillatory artery with magnetic field and heat radiation effects. With the aid of fractional time derivative, (Yakubu et al., 2021) examined the effects of pressure gradient, body acceleration, and magnetic field on blood flow through artery. The effects of blood flow parameters, Caputo's time fractional derivatives, and the external magnetic field on the cylindrical domain were studied by (Shah et al., 2016). Ali et al. (2017) solved a fractional order model for Cassons fluid flow using the Hankel transform and Laplace transform techniques to determine the exact solutions. He and collaborators (2019) used the fractional order Caputo derivative to investigate the complexity of blood in arteries under various forces. In the field of medicine, magneto hydrodynamic flow plays a crucial role. It is considered for the reduction of bleeding from wounds and for the treatment of malignant tumors. Kumar et al. (2021) employed a chemical reaction, heat source, and inclined magnetic field to cure malignancies.

The fractional order time derivative of MHD blood flow via a bifurcated artery in the presence of a slanted magnetic field, as well as the coupling impact of heat transfer and blood flow concentration, are described here using Newtonian fluid. The goal is to investigate how magneto-hydrodynamic blood flow through a bifurcated artery is affected by thermal radiation and a slanted magnetic field during tumor treatments. The Laplace transform and the indeterminate coefficients approach were used to find the exact solutions, which were then simulated to produce graphical outputs and the implications of several important parameters on the outcomes were explored. The study was motivated by the fact that there is currently very little information available on the flow in arterial bifurcation since the phenomena is currently not stringent to mathematical analysis or precise experimental measurement. The present investigation shows that the vast number of variables involved are the main challenge in both situations.

2 Methods

2.1 Physical Structure and Mathematical formulation

Blood considered in this study, is Newtonian, incompressible, homogeneous, sticky fluid that flows from the trunk to the branches. A mass stream's rate at any cross-section that is perpendicular to its direction is equal to $m = 2bv$, where b is the stream's radius and v is its mean speed. The mass stream's speed at any cross section of the extended channel is equal to $m/2$, and the bifurcating divider (internal apical curve) has no effect on this (see Figure 1). The magnetic field is applied to the flow at an angle (ϕ) since the evaluated magnetic Reynolds number is low. Therefore, it is believed that the magnetic and electric fields produced by blood flow are insignificant, the angle of bifurcation is set to zero ($\Theta = 0$), that is, the blood flow region is bifurcated into two streams that flow parallel to the principal artery (the trunk). Figure 2 demonstrates the smooth muscle fibers of the three concentric layers that make up the walls of a typical elastic artery. These fibers are controlled by the sympathetic nervous system to contract or relax.

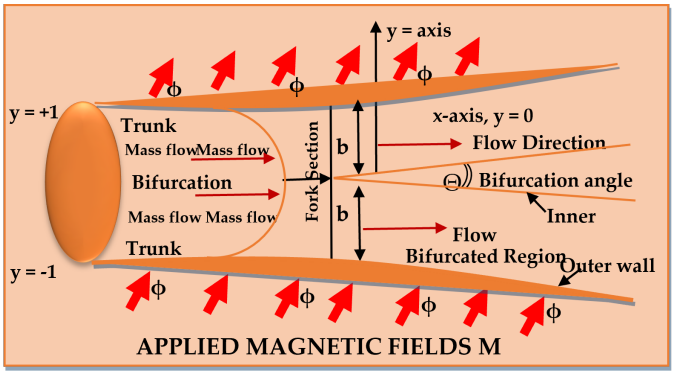

Figure 1: Physical flow diagram of the bifurcated artery with zero angle of bifurcation

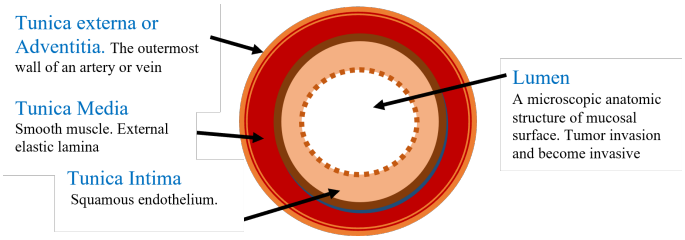

Figure 2: The structure of an artery walls (Transverse section through an artery)

2.2 Fundamental flow equations and their solutions

Blood flows through a porous media as two-limit layers when it is subjected to magnetic fields and heat, with the assumptions made in the numerical definition guiding its movement. In the stream field headings of x and y at time t , let u and v be the speed parts, η and ρ denote blood density and thickness, respectively. Blood pressure is represented by p , warm conductivity (K_T), C_p is the specific heat capacity at steady strain, hotness is represented by Q , temperature is represented by T , the volumetric development boundary is represented by β , the angle of the slanted (inclined) magnetic field is represented by ϕ, and porosity parameter is represented by K . With these, we have the equations provided by (see, Ali et al., 2017; He et al., 2019; Kumar et al., 2021), with some additional terms as follows:

$$\frac{\partial \overline{u}}{\partial \overline{t}} + \frac{1}{\rho}\frac{\partial \overline{p}}{\partial \overline{x}} = \frac{\eta}{\rho}\frac{\partial^2 \overline{u}}{\partial \overline{y}^2} + g\beta(T - T_\infty) + g\beta'(C - C_\infty) - \frac{c\mathcal{B}_\alpha^2 \sin^2\phi}{\rho}\overline{v} - \frac{\overline{v}}{\overline{k}} \tag{1}$$

$$\frac{\partial \overline{T}}{\partial \overline{t}} = \frac{\bar{k}_T}{\rho C_o}\frac{\partial^2 \overline{T}}{\partial \overline{y}^2} + \frac{Q}{\rho C_o}(T - T_o) - \frac{\partial \overline{q}}{\partial \overline{y}} \tag{2}$$

$$\frac{\partial \overline{u}}{\partial \overline{x}} + \frac{\partial \overline{v}}{\partial \overline{y}} = 0 \tag{3}$$

where, $\frac{\partial}{\partial \bar{t}}$ is the material time derivative. On the other hand, the dimensionless concentration equation for medication (concentration) delivery in magneto hydrodynamic blood flow through permeable bifurcated artery is provided by,

$$\frac{\partial \overline{C}}{\partial \overline{f}} = D\frac{\partial^2 \overline{C}}{\partial \overline{y}^2} + G \tag{4}$$

where D is the diffusion coefficient and $G = -k_1(C - C_\infty)$ represents chemical reaction rate in the fluid flow. It is important to mention that the effect of an electric field in the concentration equation was also ignored.

$$\begin{aligned} \theta = \ell^{-\bar{z}_1}, \quad u = \ell^{-\bar{z}_1}, \quad v = \ell^{-\bar{z}_1}, \quad C = \ell^{-\bar{z}_1} \quad \text{at } y = -1, \\ \text{and } \theta \to 0, \quad u \to 0, \quad v \to 0, \quad C \to 0 \quad \text{at } y = 1. \end{aligned} \tag{5}$$

However, by using the proper normalizing factors, the governing equations (1)–(4) can be converted to dimensionless form. We present the non-dimensional parameters as follows:

$$x = \frac{\bar{x}}{b}, y = \frac{\bar{y}}{b}, u = \frac{\bar{u}}{mu_{HS}/2b\rho}, \quad v = \frac{\bar{v}}{mu_{HS}/2b\rho}, h(x,t) = \frac{d\bar{p}/d\bar{x}}{u_{HS}\eta m/2b^3\rho}$$

$$\text{k}=\frac{\bar{k}}{(b^2\rho/\eta)}, C = \frac{\bar{C}\left(2b^3\rho^2\right)}{m\eta u_{HS}}, \theta = \frac{\bar{\theta}\left(2b^3\rho^2\right)}{m\eta u_{HS}}, \tau = \frac{\eta}{\rho}, \quad t = \frac{\bar{t}}{(b^2\rho/\eta)},$$

and

$$\bar{q} = \frac{-16\delta T_0^3}{3k'}\frac{\partial \bar{T}}{\partial \bar{y}} \tag{6}$$

Applying (5) and (6) to eqns. (1)- (4) and removing the bars we obtain:

$$\frac{\partial u}{\partial t} + h = \frac{\partial^2 u}{\partial y^2} + g\beta\theta + g\beta' C - M^2\sin^2\phi - \frac{u}{k} \tag{7}$$

$$\frac{\partial \theta}{\partial t} = \left(\frac{1}{\tau p_r} + R\right)\frac{\partial^2 \theta}{\partial y^2} + \left(\frac{S}{\tau p_r}\right)\theta \tag{8}$$

$$\frac{\partial u}{\partial x} + \frac{\partial v}{\partial y} = 0 \tag{9}$$

$$\frac{\partial C}{\partial t} = \frac{1}{S_C}\frac{\partial^2 C}{\partial y^2} - \omega C \tag{10}$$

where

$$M^2 = \frac{\sigma B_0^2}{\rho}, \; p_r = \frac{\rho C_\rho}{k_T}, \; R = \frac{16\delta T_0^3}{3k'\tau}, \; S = \frac{Qb^2}{k_T}, \; S_C = \frac{\tau}{bD}, \; \omega = \frac{k_1 b^2}{\tau}$$

are the magnetic field parameter, Prandtl number, thermal radiation parameter, heat source parameter, Schmidt number, chemical reaction parameter and θ is the temperature conveyance. Now, using the Caputo-Fabrizio fractional derivative as stated in (Caputo and Fabrizio 2015), we consider the time fractional momentum equations as:

$$^{CF}D_t^\alpha u(y,t) = \frac{1}{1-\alpha}\int_0^t \frac{\partial u(y,\tau)}{\partial \tau}\exp\left(-\frac{\alpha(t-\tau)}{1-\alpha}\right)d\tau, \quad 0 < \alpha < 1$$

$$L\left\{^{CF}D_t^\alpha u(y,t)\right\} = \frac{su(y,s) - u(y,0)}{(1-\alpha)s + \alpha} \tag{11}$$

$$u(y,0) = \tag{12}$$

The Caputo-Fabrizio derivative corresponding to equations (7), (8) and (10) are as follows:

$$ {}^{CF}D_t^{\alpha}u(y,t) + h = \frac{\partial^2 u}{\partial y^2} + g\beta\theta + g\beta' C - M^2 \sin^2\phi - \frac{u}{k} \tag{13} $$

$$ {}^{CF}D_t^{\alpha}\theta(y,t) = \left(\frac{1}{\tau p_r} + R\right)\frac{\partial^2\theta}{\partial y^2} + (\frac{S}{\tau p_r})\theta \tag{14} $$

$$ {}^{CF}D_t^{\alpha}C\,(y,t) = \frac{\partial C}{\partial t} = \frac{1}{S_C}\frac{\partial^2 C}{\partial y^2} - \omega C. \tag{15} $$

Applying Laplace transform to equations (13)-to-(15), and using the boundary condition in equation (12) we have;

$$ \frac{su(y,s)}{(1-\alpha)s+\alpha} + h = \frac{\partial^2\bar{u}}{\partial\bar{y}^2} + g\beta\bar{\theta} + g\beta'\bar{C} - M^2\sin^2\phi - \frac{\bar{u}}{k} \tag{16} $$

$$ \frac{su(y,s)}{(1-\alpha)s+\alpha} = \left(\frac{1}{\tau p_r} + R\right)\frac{\partial^2\bar{\theta}}{\partial\bar{y}^2} + (\frac{S}{\tau p_r})\bar{\theta} \tag{17} $$

$$ \frac{su(y,s)}{(1-\alpha)s+\alpha} = \frac{1}{S_C}\frac{\partial^2\bar{C}}{\partial\bar{y}^2} - \omega\bar{C}. \tag{18} $$

2.3 Exact solutions

Here we assume the following as the arbitrary solutions of equations (9), (16), (17) and (18),

$$ \bar{u} = \bar{F}(y)\frac{1}{s+\lambda^2}, \tag{19} $$

$$ \bar{\theta} = \bar{H}(y)\frac{1}{s+\lambda^2}, \tag{20} $$

$$ \bar{v} = \bar{G}(y)\frac{1}{s+\lambda^2}, \tag{21} $$

$$ \bar{C} = \bar{I}(y)\frac{1}{s+\lambda^2}, \tag{22} $$

then the boundary conditions in eqns. (5) reduce to;

$$ \begin{aligned} H = 1, \quad I = 1, \quad F = 1, \quad \text{at } y = -1, \\ H \to 0, \quad I \to 0, \quad F \to 0, \quad \text{at } y = 1. \end{aligned} \tag{23} $$

As a result, the following are the simplified governing equations of motions with arbitrary solutions:

$$ \frac{d^2\bar{F}}{dy^2} - A_2\bar{F} = A_3 - g\beta\bar{H} - g\beta'\bar{I}, \tag{24} $$

$$ \frac{d^2\bar{H}}{dy^2} + A_6^2\bar{H} = 0, \tag{25} $$

$$ G = A_1\,(\text{constant}), \tag{26} $$

$$ \frac{d^2\bar{I}}{dy^2} - A_9^2\bar{I} = 0. \tag{27} $$

Equation (23)'s boundary conditions are used to solve equations (24) through (27) and the following solutions are obtained:

$$ \bar{H} = \left(\frac{\cos A_6\bar{y}}{2\cos A_6}\right) - \frac{\sin A_6\bar{y}}{2\sin A_6} \tag{28} $$

$$ \bar{I} = \frac{\cosh A_9\bar{y}}{2\cosh A_9} - \frac{\sinh A_9\bar{y}}{2\sinh A_9} \tag{29} $$

$$ F = \left\{ \begin{matrix} A_7 + A\cosh A_2 y + B\sinh A_2 y + A_8\cos A_6 y + A_9\sin A_6 y + \\ + A_{10}\cosh\Lambda y + A_{11}\sinh\Lambda y \end{matrix} \right\}. \tag{30} $$

We now have blood velocity in the axial direction, using equation (30) and equation (19) as

$$ \bar{u}(y,s) = \begin{pmatrix} A_7 + A\cosh A_2\bar{y} + B\sinh A_2\bar{y} + A_8\cos A_6\bar{y} + \\ A_9\sin A_6\bar{y} + A_{10}\cosh\Lambda\bar{y} + A_{11}\sinh\Lambda\bar{y} \end{pmatrix}\frac{1}{s+\lambda^2} \tag{31} $$

Equation (26) and equation (21) together provide the usual direction of blood velocity in the bifurcated artery, which is given by

$$ \bar{v}(y,s) = A_1\frac{1}{s+\lambda^2} \tag{32} $$

According to equations (28) and (20), the temperature distribution in the bifurcated artery is given as follows:

$$ \bar{\theta}(y,s) = \left(\left(\frac{\cos A_6\bar{y}}{2\cos A_6}\right) - \frac{\sin A_6\bar{y}}{2\sin A_6}\right)\frac{1}{s+\lambda^2} \tag{33} $$

Equations (22) and (29) provide the drug's concentration in the flowing blood in the carotid artery as follows:

$$ \bar{C}(y,s) = \left(\frac{\cosh A_9\bar{y}}{2\cosh A_9} - \frac{\sinh A_9\bar{y}}{2\sinh A_9}\right)\frac{1}{s+\lambda^2}. \tag{34} $$

Equations (31) through (34) yield the inverse Laplace transform. Using Mathcad software, we simulated the given solutions using Gaver-Stehfest's algorithm, and the results are shown graphically in the next section.

3 Results and Discussion

To get the flow information, we simulated the solutions of equations (31), (33), and (34) using Mathcad software. The influence of the fractional-parameter (α) on velocity, temperature and blood concentration are displayed graphically and discussed. Axial fluid velocity, temperature distribution, and concentration are explored as functions of several dimensionless factors, including: slanted (inclined) magnetic field parameter (M), radiation parameter (R), fractional parameter (α), heat source parameter (S), and Schmidt number (S_C). In all the dimensionless parameter calculations, we vary the value of the fractional parameter (α), but we maintain other values constant, such as, $t = 1$, $S_C = 0.5$, $\omega = 0.5$, $S = 1$, $P_r = 2$, $K = 2$, $R = 0.5$, $h = 0.5$, $\beta = 0.5$, $\phi = 30^{\circ}$.

3.1 Velocity Profile

Consequently, the magnetic field always has a greater influence on the blood velocity profile. The application of the magnetic field to the system, as shown in Figure 3, increases the Lorentz force, a resistive force that primarily restricts the flow of fluid Bunonyo and Ebiwareme (2023) and Vardanyan (1973). For fractional order ($\alpha = 0.4$), as the magnetic field parameter's strength increases, as seen in Figure 3(a), the blood velocity reduces sharply, whereas it declines gradually for ($\alpha = 1$) as shown in Figure 3b.

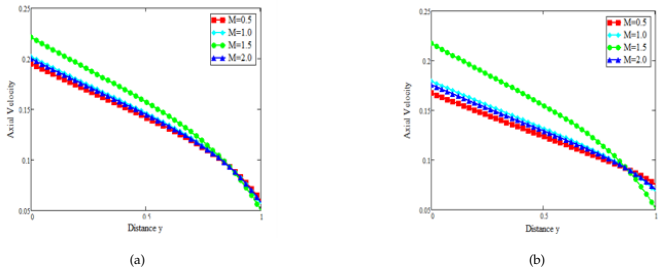

Figure 3: Axial velocity profile for different values of magnetic parameter: (a) $\alpha = 0.4$ (b) $\alpha = 1$, $\omega = 0.5$, $S = 1$, $P_r = 2$, $K = 2$, $R = 0.5$, $t = 1$, $h = 0.5$, $\beta = 0.5$, $\phi = 30°$, $Sc = 0.5$.

For therapeutic purposes and treatment procedures related to atherosclerosis, bone fractures, controlled tissue damage, and malignant tumors, to mention a few, a regulated magnetic field can therefore be a useful tool (Imoro et al., 2024). For both the fractional parameter ($\alpha = 0.4$) and the integer order model blood flow ($\alpha = 1$), Figure 4 shows the variation in blood flow at different heat source parameter (S) values. It is clear that an increase in the heat source has an impact on blood velocity and the fractional fluid parameter ($\alpha = 0.4$) (see Figure 4a). As seen in Figure 4b, the axial velocity does, however, drop symmetrically as the heat source parameter increases.

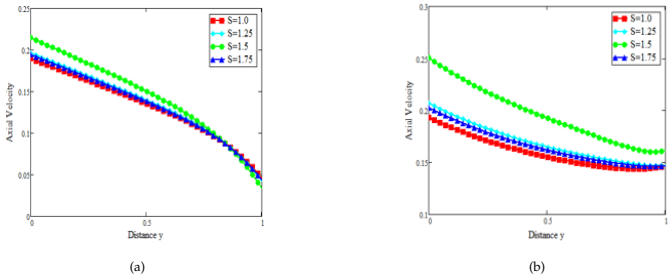

Figure 4: Profile of axial velocity for various heat source parameter: (a) $\alpha = 0.4$ (b) $\alpha = 1$, $\omega = 0.5$, $M = 0.5$, $P_r = 2$, $K = 2$, $R = 0.5$, $t = 1$, $h = 0.5$, $\beta = 0.5$, $\phi = 30°$, $Sc = 0.5$.

Figure 5 displays the velocity distribution based on different thermal radiation parameters (R). The blood velocity increases as the radiation parameter (R) increases, as indicated by both the fractional parameter ($\alpha = 0.4$) and the classical order parameter ($\alpha = 1$). Remarkably, comparable results for a related fluid model were discussed in Tabi et al. (2017). According to Yakubu et al. (2022), heat radiation possesses the capability to modify the effective viscosity of fluids, hence potentially causing an indirect influence on the velocity profile.

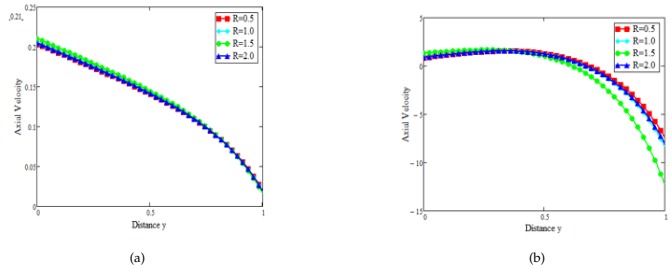

Figure 5: Profile of axial velocity for various heat source parameter: (a) $\alpha = 0.4$ (b) $\alpha = 1$, $\omega = 0.5$, $M = 0.5$, $P_r = 2$, $K = 2$, $R = 0.5$, $t = 1$, $h = 0.5$, $\beta = 0.5$, $\phi = 30°$, $Sc = 0.5$.

The applied magnetic field parameter for various tilted values is displayed in Figure 6. Blood flow is reduced over the affected area when the applied magnetic field's angle of inclination is increased for both the fractional order parameter and the classical order parameter ($\alpha = 1$). However, for the fractional order parameter in Figure 6a and 6b, the flow velocity vanishes between angles of (80° to 85°).

Because several of the related parameters' values have changed, the graphs in Figure 6c and 6d behave very differently from one another. Using Figure 6c as an example, $y = 0.004$, $p = 4$, and the fractional parameter ($\alpha = 0.2$), whereas Figure 6d also includes the fractional parameter ($\alpha = 0.4$) and $y = 0.004$, $p = 3$.

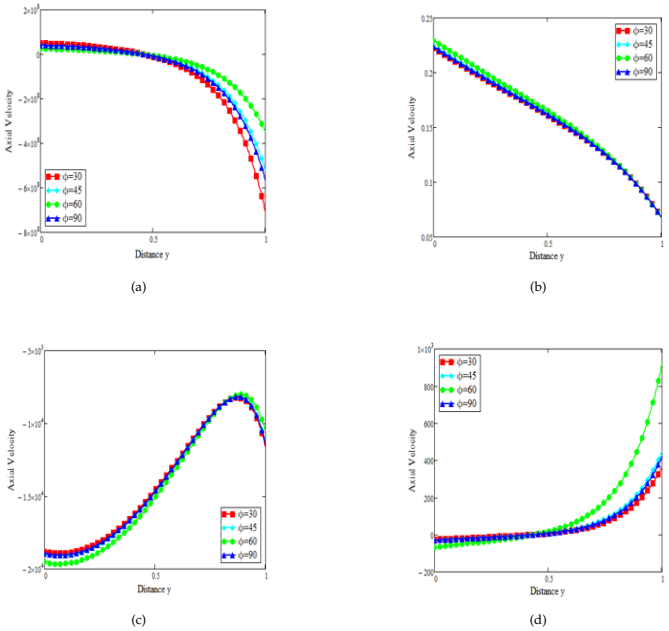

Figure 6: Axial velocity profile for various angles of inclination of the magnetic field: (a) $\alpha = 0.4$ (b) $\alpha = 1$ (c) $y = 0.004$, $p = 4$ and $\alpha = 0.2$ (d) $y = 0.004$, $p = 3$, $\alpha = 0.4$, $\omega = 0.5$, $S = 1$, $P_r = 2$, $K = 2$, $M = 0.5$, $t = 1$, $h = 0.5$, $\beta = 0.5$, $\phi = 30°$, $Sc = 0.5$.

The blood flow velocity profile at two independent times, $t = 0.01$ and 0.5, is shown in Figure 7 with five different values of the fractional parameter ($\alpha = 0.2$, 0.4, 0.6, 0.8, and 1). It has been observed that the fractional parameter (α) plays a critical role in regulating blood velocity. The fractional derivative fluid velocity initially moves faster than the integer order fluid model when the time is relatively small ($t = 0.01$). However, for a longer period of time ($t = 0.5$), the reverse behavior is seen, that is, fluids with integer order have a faster velocity than those with fractional order parameters. Naturally, this results from the system's stability, which can improve over longer timescales. For both fractional order derivative fluid models and integer order derivative fluid models, it is often observed that blood velocity increases with increasing time t. Figure 7a shows the evolution of the primary velocity profile, showing how the flow develops into fully formed Poiseuille flow, which is distinguished by the typical parabolic profile. Figure 7b clearly depicts the velocity profile at the fork section for various values of the fractional parameter. It is significant to note that when ($\alpha = 1$), a zone of sluggish flow appears along the outside wall and gets worse as time goes on, as was previously observed by Gade et al. (2026).

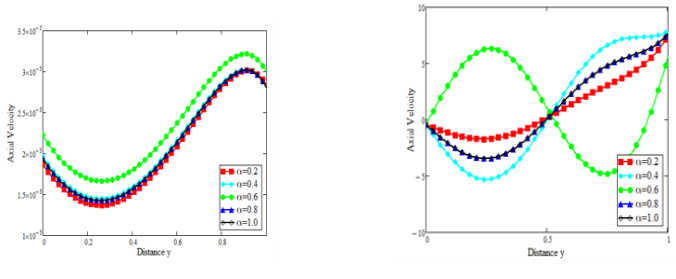

Figure 7: Axial velocity profile for different values of α at: (a) $t = 0.01$ (b) $t = 0.5$ $\omega = 0.5$, $S = 1$, $P_r = 2$, $K = 2$, $M = 0.5$, $t = 1$, $h = 0.5$, $\beta = 0.5$, $\phi = 30°$, $Sc = 0.5$

3.2 Temperature profile

Temperature profiles for different radiation parameters (R), fractional parameters , and heat source parameters (S) are shown in Figures 8–??. The temperature change for different values of the radiation parameter R, as shown in Figure 8. It is evident that when the thermal radiation increases, temperature increases for both fractional and integer order derivatives. The temperature varies near the center line for both the integer order and the fractional order derivative, as shown in Figure 8a and 8b. Consequently, it is more visible in the graphs of Figure 8b.

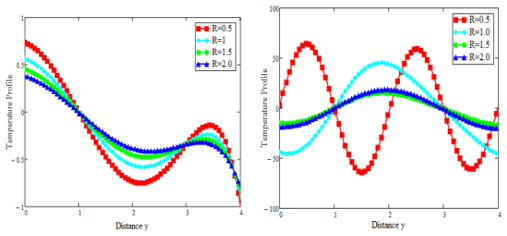

Figure 8: Temperature profile for different values of radiation parameter: (a) $\alpha = 0.4$ (b) $\alpha = 1$, $\omega = 0.5$, $S = 1$, $P_r = 2$, $K = 2$, $M = 0.5$, $t = 1$, $h = 0.5$, $\beta = 0.5$, $\phi = 30°$, $Sc = 0.5$

During hyperthermia, the temperature distribution is very important. It is commonly recognized that hyperthermia results from a breakdown in thermoregulation, which takes place when the body absorbs heat from outside sources like radiation or a body temperature that is being generated or absorbed. When a person has hyperthermia, the blood's internal temperature increases without damaging the tissues around the blood vessel. We have not taken into account the temperature exchange at the artery wall to account for this, meaning that the wall's temperature is zero. In light of this, the blood temperature in the current model is low at the artery wall and high at the midline for classical fluid. Numerous theoretical and experimental studies for Newtonian and non-Newtonian fluids of integer order reported similar phenomena, for example in (Ramesh & Devakar, 2015). Similar to radiation, the heat source (S) another crucial factor, has a large impact on the bloodstream's temperature distribution. More mitochondria per cell increase the thermal activity involved with the heat production process, as seen in Figure 9, which raises the system's temperature. The heat source improves the temperature distribution and supplies more heat to the blood flow system even though the wall temperature must remain zero in order to meet the boundary conditions. The temperature distribution at the channel walls, which decreases and becomes more flattened toward the channel's center line when the heat source is increased as shown in Figure 9a, which is amplified to maintain a constant flow rate, as seen in Figure 9a

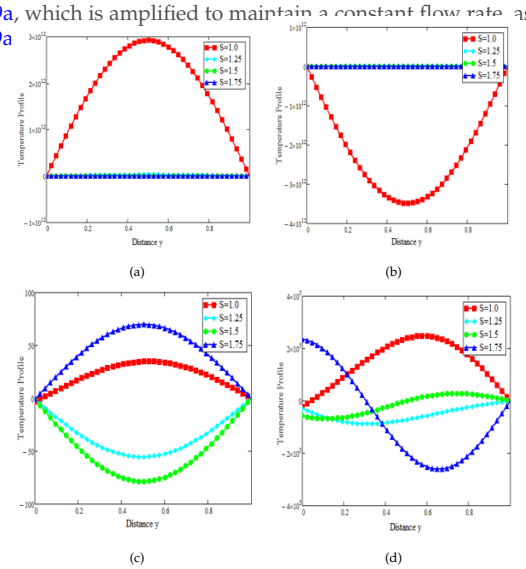

Figure 9: Temperature profile for different values of heat source parameter: (a) $\alpha = 0.4$ (b) $\alpha = 1$, $\omega = 0.5$, $R = 0.5$, $P_r = 2$, $K = 2$, $M = 0.5$, $t = 1$, $h = 0.5$, $\beta = 0.5$, $\phi = 30°$, $Sc = 0.5$

It's noteworthy to see in Figure 9b that the temperature at the middle line of the channel decreases as the heat source's values rise. The temperature exhibits oscillating behavior for different amounts of the heat source in Figures 9c and 9d. As the values of the heat source rise, the temperature is maximum at the center, decreases, and finally approaches zero at the artery walls. The different values of the fractional parameter really cause a shift in the temperature distribution, as shown in Figure 10. It illustrates how temperature increases with increasing fractional parameter . This implies that the fractional order fluid model's temperature distribution is more faster and higher over a longer period of time, which is what causes the variation shown in Figures 10a and 10b, as mentioned earlier. The temperature gradually decreases toward the artery's axis in Figures 10c and 10d, eventually tending to align with the axis.

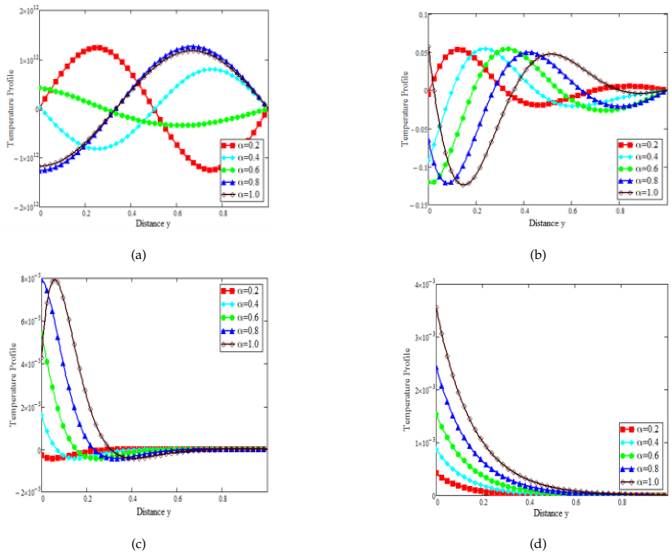

Figure 10: Temperature profile for different values of α at: (a) $t = 0.05$, $y = 0.004$, $p = 1$ and $\alpha = 1$, $t = 0.1$ (b) $t = 0.25$, $\omega = 0.5$, $S = 1$, $P_r = 2$, $K = 2$, $M = 0.5$, $t = 1$, $h = 0.5$, $\beta = 0.5$, $\phi = 30°$, $Sc = 0.5$, $y = 0.004$, $p = 3$, $\alpha = 0.4$. (c) $y = 0.004$, $p = 2$ and $\alpha = 1$, $t = 0.1$ (d) $y = 0.004$, $p = 10$, $\alpha = 0.01$, $t = 0.1$.

3.3 Concentration profile

The concentration profile for different values of fractional order parameter (α) , Schmidt number (Cs) , and chemical process (ω) is shown in Figures 11 to 13. There is a relationship between the blood concentration and the quantity of blood cells floating in the plasma. Red blood cells (RBCs) are important blood cells because of their size and density in the bloodstream. RBCs assembled at the center of the vessel, where there is a greater concentration of solutes, due to their revolving nature. However, because the off-axis zone is an area predominantly represented by cells that carry plasma, the solute concentration there decreases to a minimum. This observation is displayed in all of the concentration graphs in this section. The fractional model fluid in Figure 11 reaches a greater concentration more quickly than the integer order fluid (Imoro et al., 2024).

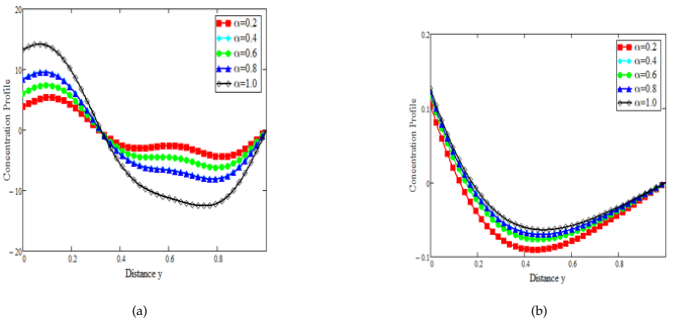

Figure 11: Concentration profile for different values of α at: (a) $t = 0.1$ (b) $t = 0.5$ $Sc = 0.5$, $S = 1$, $R = 0.5$, $P_r = 2$, $K = 2$, $M = 0.5$, $t = 1$, $h = 0.5$, $\beta = 0.5$, $\phi = 30°$

This is because a fractional order derivative that restricts fluid flow is included in the model. The Schmidt number exhibits the opposite pattern. The blood cells show an additional force of the temperature gradient in the presence of the Schmidt number, as seen in Figure 12, which further increases the concentration. Therefore, lower Schmidt number values, for example in industrial applications, physically represent hydrogen gas as the species diffusing (Sademaki et al., 2026).

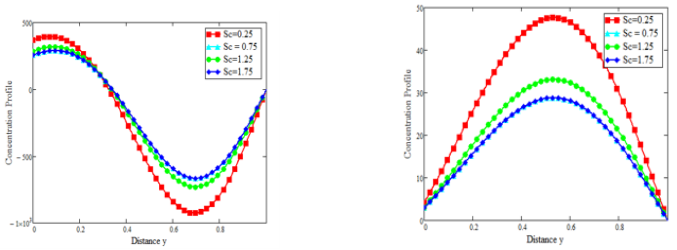

Figure 12: Concentration profile for different values of Schmidt number: (a) $\alpha = 0.4$ (b) $\alpha = 1$, $\omega = 0.5$, $S = 1$, $R = 0.5$, $P_r = 2$, $K = 2$, $M = 0.5$, $t = 1$, $h = 0.5$, $\beta = 0.5$, $\phi = 30^\circ$

Figure 12 illustrates how the species' chemical molecular diffusivity decreases dramatically with increasing Schmidt number (Sc) , making it easier for the species to enter the flow field and raising the mass transfer function. Higher Schmidt number compounds can enhance mass transfer and dispersion properties in the bloodstream, especially for pharmaceutical diffusion in pulse blood flow. The amplitude of the blood flow concentration is larger for the integer order derivative. As demonstrated in Figure 13a and 13b, this phenomena is clearly seen along the flow axis $(0 \leq y \leq 0.5)$ and slowly declines in the region $(0 \leq y \leq 1)$ for both fractional and integer order derivatives, respectively. As can be observed from all of the graphs in Figure 13, the blood flow decreases along the distensible tube's length where the graphs begin to fluctuate because of the size of the chemical reaction parameter's peak value (pressure gradient) (see, Abdul-Wahab & Al-Saif, 2024). Furthermore, it has been demonstrated that the variation is more pronounced in the larger section of the artery wall, permitting the flow to pass without producing a perceptible pressure gradient. Nevertheless, the substantial pressure gradient is usually required to maintain a consistent flow rate as it passes through the constrictions in the artery.

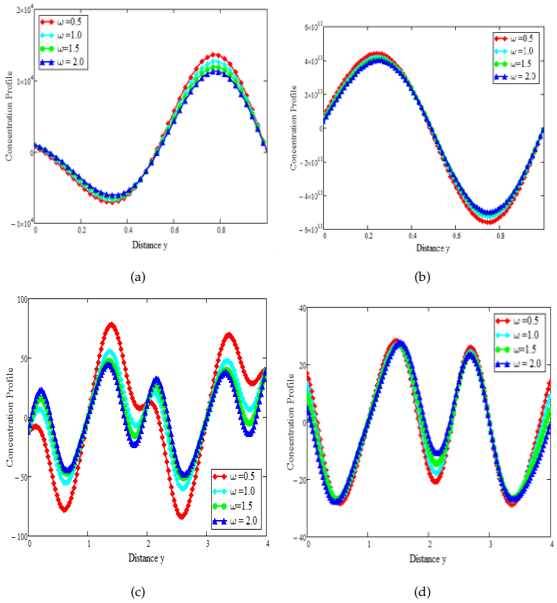

Figure 13: Concentration profile for different values of the chemical reaction parameter: $Sc = 0.5$, $S = 1$, $P_r = 2$, $K = 2$, $M = 0.5$, $t = 1$, $h = 0.5$, $\beta = 0.5$, $\phi = 30^\circ$, $R = 0.5$ (a) $\alpha = 0.4$ (b) $\alpha = 1$.

4 Conclusion

Currently, a fractional-order model of the magneto hydrodynamic blood flow via a bifurcated artery under the influence of thermal radiation, a slanted magnetic field, and a heat source during tumor treatment is being developed. The Laplace transform and the combined methods of indeterminate coefficients were used to solve the mathematical models. The fractional order parameter has a major effect on the blood velocity profiles, concentration, and temperature distribution. It has been noted that fluids with fractional order can occasionally move faster than those with integer order. Fractional model fluid flow is slower than integer-order fluid flow over longer dimensionless durations. The impact of fluid velocity is demonstrated by the fact that the rate of increase in fluid velocity is slower at larger levels of the magnetic field parameter. As the chemical reaction parameter rises, the blood flow concentration falls. The blood concentration rises as the Schmidt number rises. As the fractional parameter and the heat source increase, the blood flow's dimensionless temperature rises, which also affects the radiation parameter. We noted that the outcomes will be intriguing to comprehend and evaluate throughout cancer therapy using hyperthermia. Additionally, it will be useful in understanding the drug particle concentration phenomena for applications and administrations involving drug delivery. Our research's findings should serve as a foundation for the study of increasingly sophisticated blood flow models and also serve as a basis for in vitro and in vivo testing, particularly in the application areas like medicine, biomedical engineering, biology, pathology, and other related domains.

Acknowledgments

This work was supported by Tertiary Education Trust Fund (TETFund) Ref. No. TETF/ DR&D/CE /UNI /BAUCHI /IBR /2025/ VOL.1. Therefore, the authors gratefully acknowledged the financial support of the TETFUND. The authors would like to express their sincere gratitude to the handily editor and the reviewers for their helpful and informative comments, which have enhanced the manuscript.

Declaration of Generative AI

The authors declare that they do not used generative AI in the scientific writing.

References

Abdulhameed, M., Babagana, B., Markus, S., Yakubu, D. G., & Adamu, G. T. (2023). The effects of fractional relaxation time and magnetic field on blood flow through arteries along with nanoparticles. *Defect and Diffusion Forum*, *424*, 59–76.

Abdulhameed, M., Vieru, D., & Roslan, R. (2017). Modeling electro-magnetohydrodynamic thermo-fluidic transport of biofluids with new trend of fractional derivative without singular kernel. *Physica A*, *484*, 233–252.

Abdul-Wahab, M. S., & Al-Saif, A. S. J. A. (2024). A new method for studying blood flow through stenotic artery in the presence of a magnetic field. *Intern. J. Appl. Comput. Math.*, *10*(49). https://doi.org/10.1007/s40819-024-01684-x

Akbar, N. S., & Butt, A. W. (2017). Entropy generation analysis in convective ferromagnetic nano blood flow through a composite stenosed arteries with permeable wall. *Commun. Theor. Phys.*, *67*, 554–560.

Ali, F., Sheikh, N. A., Khan, I., & Saqib, M. (2017). Magnetic field effect on blood flow of casson fluid in axisymmetric cylindrical tube: A fractional model. *J. Magn. Magn. Mater.*, *423*, 327–336.

Atangana, A., & Baleanu, D. (2016). New fractional derivative with non-local and non-singular kernel: Theory and application to heat transfer model. *Thermal Science*, *21*(2), 761–766. https://doi.org/10.2298/TSCI160517180A

Bansi, C. D. K., Tabi, C. B., Motsumi, T. G., & Mohamadoud, A. (2018). Fractional blood flow in oscillatory arteries with thermal radiation and magnetic field effects. *J. Magn. Magn. Mater.*, *456*, 38–45.

Bhargava, R., Rawat, S., Takhar, H. S., & Bég, O. A. (2007). Pulsatile magnetobiofluid flow and mass transfer in a non-darcian porous medium channels. *Meccanica*, *42*, 247–262.

Bhatti, M. M., & Lu, D. Q. (2019). Analytical study of the head-on collision process between hydroelastic solitary waves in the presence of a uniform current. *Symmetry*, *11*, 333.

Bhatti, M. M., Zeeshan, A., & Ellahi, R. (2016). Heat transfer analysis on peristaltically induced motion of particle-fluid suspension with variable viscosity: Clot blood model. *Comput. Math. Prog. Biomed.*, *137*, 115–124.

Bhatti, M. M., Zeeshan, A., Ellahi, R., & Shit, G. C. (2018). Mathematical modeling of heat and mass transfer effects on MHD peristaltic propulsion of two-phase flow through a Darcy-Brinkman-Forchheimer porous medium. *Adv. Powder Tech.*, *29*, 1189–1197.

Bunonyo, K. W., & Ebiwareme, L. (2023). Mathematical analysis of a magnetic and conducting fluid flow through blood vessel along with an inclination and chemical radiation. *European J. Theoretical and Applied Sciences*, *1*(6), 3–15.

Caputo, M., & Fabrizio, M. (2015). A new definition of fractional derivative without singular kernel. *Progress in Fractional Differentiation and Applications*, *1*(2), 73–85.

Caro, C. G., Pedley, T. J., Schroter, R. C., & Seed, W. A. (2011). *The mechanics of the circulation*. Cambridge University Press.

Chaturani, P., & Palanisamy, V. (1990). Casson fluid model for pulsatile flow of blood under periodic body acceleration. *Biorheology*, *27*(5), 619–630.

Chinyoka, T., & Makinde, O. D. (2014). Computational dynamics of arterial blood flow in the presence of magnetic field and thermal radiation therapy. *Adv. Math. Phys.*, *2014*, 915640.

Dash, R. K., Mehta, K. N., & Jayaraman, G. (1996). Casson fluid flow in a pipe filled with homogeneous porous medium. *Int. J. Engg. Sci.*, *34*, 1146–1156.

Gade, M. R., Kalakuntla, S. R., Adigoppula, R., & Itikela, S. (2026). Prediction of micropolar fluid flow characteristics in a stenosed bifurcated artery using feed-forward neural networks trained by the Levenberg Marquardt Algorithm. *Partial Diff. Equat. Appl. Math.*, *18*, 101366.

Ghasemi, S. E., Hatami, M., Hatami, J., Sahebi, S. A. R., & Ganji, D. D. (2016). An efficient approach to study the pulsatile blood flow in femoral and coronary arteries by differential quadrature method. *Physica A*, *443*, 406–414.

Ghasemi, S. E., Hatami, M., Sarokolaie, A. K., & Ganji, D. D. (2015). Study on blood flow containing nanoparticles through porous arteries in presence of magnetic field using analytical methods. *Physica E*, *70*, 146–156.

Hayat, T., Asad, S., & Alsaedi, A. (2016). Flow of casson fluid with nanoparticles. *Appl. Math. Mech.*, *37*(4), 479–470.

He, S., Fataf, N. A. A., Banerjee, S., & Sun, K. (2019). Complexity in the muscular blood vessel model with variable fractional derivative and external disturbances. *Physica A*, *526*, 120904.

Imoro, I., Etwire, C. J., & Musah, R. (2024). MHD flow of blood-based hybrid nanofluid through a stenosed artery with thermal radiation effect. *Case Studies in Thermal Engin.*, *59*, 104418.

Kumar, D., Satyanarayana, B., Rajesh, K., Narendra, D., & Sanjeev, K. (2021). Application of heat source and chemical reaction in magnetohydrodynamic blood flow through permeable bifurcated arteries with inclined magnetic field in tumor treatments [1-13]. *Results in Applied Mathematics*, *10*, 100151.

Liepsch, D. (1986). Flow in tubes and arteries - A comparison. *Biorheology*, *23*, 395–433.

MacDonald, D. A. (1979). On steady flow through modeled vascular stenosis. *J. Biomech.*, *12*(1), 13–20.

Majee, S., & Shit, G. C. (2017). Numerical investigation of MHD flow of blood and heat transfer in a stenosed arterial segment. *J. Magn. Magn. Mater.*, *424*, 137–147.

Misra, J. C., & Shit, G. C. (2009). Flow of a biomagnatic visco-elastic fluid in a channel with stretching walls. *J. Appl. Mech.*, *76*(6), 061006.

Mondal, A., & Shit, G. C. (2017). Transport of magneto-nanoparticles drugging electro-osmotic flow in a micro-tube in the presence of magnetic field for drug delivery application. *J. Magn. Magn. Mater.*, *442*, 319–328.

Nagarani, P., Sarojamma, G., & Jayaraman, G. (2006). Exact analysis of unsteady convective diffusion in casson fluid flow in an annulus-Application to catheterized artery. *Acta Mechanica*, *187*, 189–202.

Prasad, K. V., Vaidya, H., Choudhari, R., Tripathi, D., Karanth, S., & Hanumantha. (2025). Advancing blood flow in stenotic arteries through magnetohydrodynamic peristaltic motion of hybrid nanoparticles. *Chinese Journal of Physics*, *96*, 1144–1163.

Ramesh, K., & Devakar, M. (2015). Magneto hydrodynamic peristaltic transport of couple stress fluid through porous medium in an inclined asymmetric channel with heat transfer. *J. Magn. Magn. Mater.*, *394*, 335–348.

Sademaki, L. J., Reddy, B. P., & Matao, P. M. (2026). Dissipative and radiative consequences on diffusional reactive MHD nanofluid flow over an inclined vertical cone in a porous medium with reactive species: FEM study. *Partial Diff. Equat. Appl. Math.*, *18*, 101365.

Samko, S. G., Kilbas, A. A., & Marichev, O. I. (1993). *Fractional integrals and derivatives: Theory and applications*. Gordon; Breach Science Publishers.

Shah, N. A., Vieru, D., & Fetecau, C. (2016). Effects of the fractional order and magnetic field on the blood flow in cylindrical domains. *J. Magn. Magn. Mater.*, *409*, 10–19.

Shaw, S., & Murthy, P. V. S. N. (2010). Magnetic drug targeting in the permeable blood vessel - The effect of blood rheology. *J. Nanotechnol. Eng. Med.*, *1*(2), 021001–11.

Shit, G. C., & Majee, S. (2015). Pulsatile flow of blood and heat transfer with variable viscosity under magnetic and vibration environment. *J. Magn. Magn. Mater.*, *388*, 106–115.

Shit, G. C., & Roy, M. (2015). Effect of slip velocity on peristaltic transport of a magneto-micropolar fluid through a porous non-uniform channel. *Int. J. App. Compt. Math.*, *1*, 121–141.

Sinha, A., & Shit, G. C. (2015). Electromagnetohydrodynamic flow of blood and heat transfer in a capillary with thermal radiation. *J. Magn. Magn. Mater.*, *378*, 143–151.

Srivastava, L., & Srivastava, V. (1984). Peristaltic transport of blood: Casson model-11. *J. Biomech.*, *17*(11), 821–829.

Sud, V. K., & Sekhon, G. S. (1984). Blood flow subject to a single cycle of body acceleration. *Bull. Math. Biol*, *46*, 937–949.

Syed, M. H., Mustansar, S. H. S., Hijaz, A., Nazar, T., Wasim, J., Mohamed, R. E., et al. (2026). Thermal characteristics of magnetic blood-based hexa-hybrid nanofluids in stenotic arteries with heat source/sink by applying Caputo-Fabrizio fractional derivatives [In Press]. *Results in Surfaces and Interfaces*.

Tabi, C. B., Motsumi, T. G., Kamdem, C. D. B., & Mohamadou, A. (2017). Nonlinear excitations of blood flow in large vessels under thermal radiations and uniform magnetic field. *Commun. Nonl. Sci. Numer. Simul.*, *49*, 1–8.

Tzirtzilakis, E. E. (2005). A mathematical model for blood flow in magnetic field. *Phys. Fluids*, *17*(7), 077103.

Vardanyan, V. A. (1973). Effect of magnetic field on blood flow. *Biofizika*, *18*, 491–496.

Venkatesan, J., Sankar, D., Hemalatha, K., & Yatim, Y. (2013). Mathematical analysis of casson fluid model for blood rheology in stenosed narrow arteries. *J. Appl. Math.*, *2013*, 1–11.

Yakubu, D. G., Abdulhameed, M., Adamu, G. T., & Kwami, A. M. (2020). A study of fractional relaxation time on blood flow in arteries with magnetic radiation effects. *Diff. Found.*, *26*, 126–144.

Yakubu, D. G., Abdulhameed, M., Adamu, G. T., Roslan, R., Issakhov, A., Rahimi-Gorji, M., & Bakouri, M. (2021). Towards the exact solution of Burger's fluid flow through arteries with fractional time derivative magnetic field and thermal radiation effects. *J. Proce. Mech. Eng.*, *235*, 1618–1627.

Yakubu, D. G., Mohammed, A., Garba, T. A., Usman, H., & Muhammad, L. K. (2022). Construction of the exact solution of blood flow of Oldroyd-B fluids through arteries with effects of fractional derivative magnetic field and heat transfer. *J. Mech. Med. Biol.*, *22*(10), 2250068.

Zeeshan, A., Bhatti, M. M., Akbar, N. S., & Sajjad, Y. (2017). Hydromagnetic blood flow of Sisko-fluid in a non-uniform channel induced by peristaltic wave. *Commun. Theor. Phys.*, *68*, 103–110.

Appendix

$$A_1 = 1, \quad A_2 = M^2 \sin^2\phi - \frac{1}{k} - \frac{s}{(1-\alpha)s+\alpha}, \quad A_3 = h(s+\lambda^2), \quad A_4 = \frac{\tau p_r}{R\tau p_r + 1},$$

$$A_3 = h(s+\lambda^2), \quad A_4 = \frac{\tau p_r}{R\tau p_r + 1}, \quad A_5 = \left(\frac{S}{\tau p_r} - \frac{S}{(1-\alpha)s+\alpha}\right)(s+\lambda^2), \quad A_6 = \sqrt{A_4 A_5}, \quad A_7 = \frac{A_3}{A},$$

$$A_9 = \sqrt{Sc(\omega + s((1-\alpha)s+\alpha))}, \quad A_{10} = \frac{-g\beta}{2(A_9^2 - A_2)\cosh A_9}, \quad A_{11} = \frac{g\beta}{2(A_9^2 - A_2)\sinh A_9}$$